Available online at www.sciencedirect.com
SCIENCE DIRECT®
Journal of Catalysis 231 (2005) 381–392
JOURNAL OF CATALYSIS
www.elsevier.com/locate/jcat

Synthesis and characterization of CuMgAl ternary hydrotalcites as catalysts for the hydroxylation of phenol

S. Kannan [a,*], A. Dubey [a,1], H. Knozinger [b]

[a] *Silicates and Catalysis Discipline, Central Salt and Marine Chemicals Research Institute, Bhavnagar-364 002, India*
[b] *Department Chemie, Physikalische Chemie, LMU München, Butenandtstrasse 5-13 (Haus E), 81377 München, Germany*

Received 23 November 2004; revised 24 January 2005; accepted 31 January 2005

Available online 23 March 2005

Abstract

CuMgAl ternary hydrotalcites with a (Cu + Mg)/Al atomic ratio of 3.0 and a Cu/Mg atomic ratio of 5.0, 3.0, 1.0, 0.33, and 0.2 were synthesized by coprecipitation under low supersaturation. Powder X-ray diffraction (PXRD) of all of the samples showed the pattern characteristic of hydrotalcite without any detectable impurity phases, with the crystalline order, especially in the *ab* plane, improving with an increase in magnesium concentration. In situ PXRD studies revealed varying phase evolution processes depending on the concentration of magnesium; this observation was well complemented by in situ diffuse reflectance infrared Fourier transform (DRIFT) measurements. The thermal stability of these materials also improved with an increase in magnesium concentration, as indicated by TG-DTA-EGA measurements. However, a characteristic endotherm was noted at temperatures around 870 K accompanied by the evolution of CO_2, the intensity of which increased with an increase in copper concentration. Catechol (CAT) and hydroquinone (HQ) were the main products noted in the hydroxylation of phenol over these materials, with H_2O_2 as oxidant and H_2O as solvent. Variation of the substrate:catalyst mass ratio (10–500) showed that the activity passes through a maximum for a ratio of 100. The influence of reaction time indicated that the reaction was nearly complete in less than 60 min. Activity was enhanced by an increase in the concentration of copper, whereas the normalized activity (activity per unit copper concentration) showed an opposite trend. The structure–activity relationship of these samples, obtained through scanning electron microscopy, N_2 adsorption measurements, X-ray photoelectron spectroscopy, and cyclic temperature-programmed reduction–oxidation measurements, corroborated such activity variations.

Keywords: CuMgAl ternary hydrotalcite; Hydroxylation of phenol; In situ PXRD; DRIFT spectroscopy; Structure–activity relationships; Cyclic TPR-TPO measurements; Dispersion

1. Introduction

Hydrotalcite-like compounds comprise a class of anionic clays or layered double hydroxides that have received increasing attention in recent years because of their diverse applications as ion exchangers [1,2], catalysts [3–5], catalyst supports [6], and polymer additives [7]. Structurally, they can be understood from an examination of the brucite [$(Mg(OH)_2)$] lattice, wherein a partial replacement of Mg^{2+} with a trivalent cation, say Al^{3+}, occurs, and the resulting excess positive charge is compensated for by anions, usually carbonate, occupying interlayer positions. Synthesis of these materials containing transition metal ions, especially copper, in the sheets is of particular interest because of their selective oxidation properties.

Hydroxylation of phenol to dihydroxybenzenes (Scheme 1) is an important selective oxidation reaction whose products, catechol and hydroquinone, are used in such diverse applications as photographic chemicals, antioxidants, flavoring agents, polymerization inhibitors and pharmaceuticals. In a recent study, we reported on the hydroxylation

* Corresponding author.
E-mail address: kanhemad1@sancharnet.in (S. Kannan).
[1] Present address: Department of Chemistry, Korea Advanced Institute of Science and Technology, Taejon, 305-701, Korea.

0021-9517/$ – see front matter
doi:10.1016/j.jcat.2005.01.032

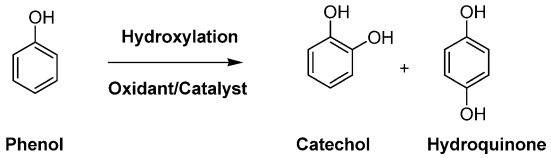

Scheme 1. Hydroxylation of phenol.

of phenol over various copper-containing ternary hydrotalcites containing different di- and trivalent metal ions and that these materials have activities comparable to those of some of the zeolite-based materials [8–10]. In the present study, magnesium was chosen as a second divalent cation in CuMgAl ternary hydrotalcites with the goal of elucidating the influence of divalent non-transition-metal cation on their catalytic performance.

Corma and co-workers [11] reported that a catalyst with a Cu/Mg atomic ratio of 1, which was obtained by calcination and reduction of a CuMgAl hydrotalcite, was active in the selective catalytic reduction of NO by propane and in the SO_x removal from exhaust streams. Auer et al. [12] have studied the synthesis of methyl amines with the use of mixed-metal oxides derived from CuMgAl hydroxy carbonates with different Mg/Al atomic ratios and observed maximum activity for a precursor composition for which a pure HT-like phase was detected. The presence of copper also strongly enhanced the activity of mixed oxides prepared from CuMgAl oxides (33 at% Cu) for the oxidation of ammonia with high selectivity toward nitrogen and the SCR activity (NO by NH_3), whereas the binary MgAl oxide catalyst did not show any measurable SCR activity under similar conditions and produced significant amounts of nitrogen oxides during ammonia oxidation [13]. Recently, Kaneda and co-workers [14] reported that an alkali-promoted CuMgAl hydrotalcite (a Cu/Mg atomic ratio of 1:10 and a (Cu + Mg)/Al ratio of nearly 3.0) was active for the selective oxidation of 2,6-di-*tert*-butylphenol to 3,3′,5,5′-tetra-*tert*-butyl-4,4′-diphenoquinone, with molecular oxygen as the oxidant. The authors claimed that both Cu^{2+} and the base were essential to this reaction.

Although scattered information on CuMgAl hydrotalcites is available, a systematic investigation of the effect of the variation of the Cu/Mg atomic ratio in CuMgAl hydrotalcites on their properties for selective catalytic oxidations is still lacking. Therefore, we report here on the catalytic performance of a series of CuMgAl ternary hydrotalcites with varying Cu/Mg atomic ratios for the selective hydroxylation of phenol with H_2O_2 as the oxidant in aqueous solution.

2. Experimental

2.1. Sample preparation

All chemicals were from S.D. Fine Chemicals (India). The samples were prepared by the low supersaturation technique. Two solutions, one (A) containing the desired amount of metal (Cu, Mg, Al) nitrates and one (B) with precipitating agents (i.e., NaOH and Na_2CO_3), were added simultaneously, while the pH was maintained around 9–10 under vigorous stirring at room temperature. The addition took ca. 90 min and the final pH was adjusted to 10. The samples were aged in the mother liquor at 338 K for 24 h, filtered off, washed (until the total absence of nitrates and sodium), and dried in air at 353 K for 12 h. The resulting solids were ground in a mortar. They exhibited a grayish blue to light blue color. In all cases, the atomic ratio between the divalent and trivalent cations was maintained around 3.0, while the Cu/Mg atomic ratio was varied between 5:1 and 1:5. The samples are denoted CuMgAl-XY, where XY stands for the nominal Cu/Mg atomic ratio.

2.2. Experimental techniques

2.2.1. Chemical analysis

Elemental chemical analysis for Cu, Mg, and Al was carried out with inductively coupled plasma (ICP) spectrometry (Varian Vista RL CCD) in which the samples were digested in a microwave oven with small quantities of a mixture of HNO_3 and HF.

2.2.2. Powder X-ray diffraction

Powder X-ray diffraction was carried out in a Philips X'Pert MPD system with Cu-K_α radiation ($\lambda = 1.54056$ Å). A step size of 0.14° and a step time of 5.6 s were used for data collection. The data were processed with Philips X'Pert (version 1.2) software. The operating voltage and the current were 40 kV and 40 mA, respectively. In situ powder X-ray diffraction (PXRD) was carried out on the same system connected to an Anton–Paar high-temperature XRK assembly in which the sample was mounted in a high-temperature cell, heated at 5 K min^{-1} in steps of 50 K, and stabilized for 5 min before measurements. The step size was 0.05° with a step time of 1 s. Identification of the crystalline phases was made by comparison with the JCPDS files [15].

2.2.3. Diffuse reflectance infrared spectroscopy

DRIFT measurements (with variable temperature programming) were carried out with the use of a self-supporting disc in a Perkin–Elmer FT1730 spectrometer connected to a diffuse reflectance accessory (Graseby Specac, USA; P/N 19930 series). Background corrections were made with KBr as a reference prior to measurements, and we recorded the spectra by accumulating 64 scans at a spectral resolution of 2 cm^{-1}.

2.2.4. Thermogravimetry and differential thermal analysis

Thermogravimetry-differential thermal analysis (TG-DTA) was carried out on a Netzsch STA 409 thermobalance. Analysis was done from 323 to 973 K at a heating rate of 10 K min^{-1} under nitrogen (30 cc min^{-1}). The gases evolved during the thermal treatment, H_2O ($m/e = 18$) and CO_2

Table 1
Elemental analysis, chemical formulae and lattice parameters of the samples synthesized

Sample	M(II)/Al[a]		Cu/Mg[a]		Formula[b]	*a* (Å)	*c* (Å)
	Solution	Solid	Solution	Solid			
CuMgAl-51	3.0	3.06	5.0	5.18	$[Cu_{0.63}Mg_{0.12}Al_{0.25}(OH)_2](CO_3)_{0.13}\cdot 0.58H_2O$	Nd[c]	22.70
CuMgAl-31	3.0	3.02	3.0	2.95	$[Cu_{0.56}Mg_{0.19}Al_{0.25}(OH)_2](CO_3)_{0.13}\cdot 0.61H_2O$	3.080	22.76
CuMgAl-11	3.0	3.08	1.0	0.99	$[Cu_{0.37}Mg_{0.38}Al_{0.25}(OH)_2](CO_3)_{0.13}\cdot 0.67H_2O$	3.070	22.87
CuMgAl-13	3.0	3.04	0.33	0.32	$[Cu_{0.18}Mg_{0.57}Al_{0.25}(OH)_2](CO_3)_{0.13}\cdot 0.68H_2O$	3.063	22.95
CuMgAl-15	3.0	3.07	0.20	0.19	$[Cu_{0.12}Mg_{0.63}Al_{0.25}(OH)_2](CO_3)_{0.13}\cdot 0.70H_2O$	3.067	23.18

[a] Atomic ratio.
[b] Values rounded to two significant figures.
[c] Not determined.

($m/e = 44$), were simultaneously analyzed with an on-line quadruple mass spectrometer (Balzers QMG 4211).

2.2.5. Temperature-programmed reduction and reoxidation

Cyclic temperature-programmed reduction–reoxidation (TPRO) measurements were carried out in a custom-designed system with He as carrier gas and a thermal conductivity detector (TCD). High-purity oxygen (99.99%; 5% in He) and hydrogen (99.99%; 5% in He) were premixed with helium with the use of mass flow controllers (Brooks Model 5600). Sample weights were taken so as to fulfil the Monti and Baiker criterion [16] and were heated under both reducing and oxidizing atmospheres from room temperature to 1073 K at a heating rate of 10 K min^{-1}. Calibration of the instrument was carried out with CuO (Merck).

2.2.6. X-ray photoelectron spectroscopy

X-ray photoelectron spectroscopy was carried out on an ESCALAB (VG Scientific, UK). The sample was pressed as a disk and measured, with Mg-K_α radiation (1253.6 eV) as the excitation source. The vacuum during measurements was better than 5×10^{-8} mbar, and the data were analyzed with the use of standard software. The binding energy scale was calibrated with respect to the adventitious carbon (C 1s) at 284.6 eV.

2.2.7. Scanning electron microscopy

Scanning electron micrographs were obtained with a Leo (Model 1430) microscope operating at an acceleration voltage of 15 kV and a working distance of 17 mm, with magnification values up to 100,000×.

2.2.8. Surface area measurements

The specific surface areas and pore size distribution of the samples were measured by nitrogen adsorption at 77 K with a sorptometer (ASAP-2010, Micromeritics). The samples were degassed at 393 K for 4 h prior to measurements.

2.2.9. Catalytic activity measurements

The hydroxylation of phenol in aqueous solution was carried out in a two-necked glass reactor (50 ml) fitted with a condenser and a septum. Hydrogen peroxide (30% v/v) was added through the septum to the magnetically stirred solution of phenol containing the catalyst and kept at the desired reaction temperature. We monitored the course of the reaction by periodically taking small samples (0.05 cm^3), which were analyzed by gas chromatography (GC) (Shimadzu-14B) with a OV-17 packed column (2 m, 4 mm i.d.) and a flame ionization detector. Quantification was done after we considered the response factors of reactants and products, the retention times of which were determined from authentic samples, which were derived from standard mixtures containing both of them.

3. Results and discussion

3.1. Catalyst characterization

Table 1 summarizes the elemental compositions and the formulas calculated for the samples studied. The carbonate content was calculated based on the M(II)/Al atomic ratio, and the water content was computed based on thermogravimetric results. A reasonable coincidence was noted between the solution concentrations with those of solids, suggesting completion of precipitation; the small deviation observed is rather common and has usually been attributed to a preferential precipitation of one or another metal ion as a hydroxide.

Powder X-ray diffraction patterns for all of the samples are shown in Fig. 1. Sharp, intense peaks at low diffraction angles (peaks close to $2\theta = 11°$, 24°, and 35°; ascribed to

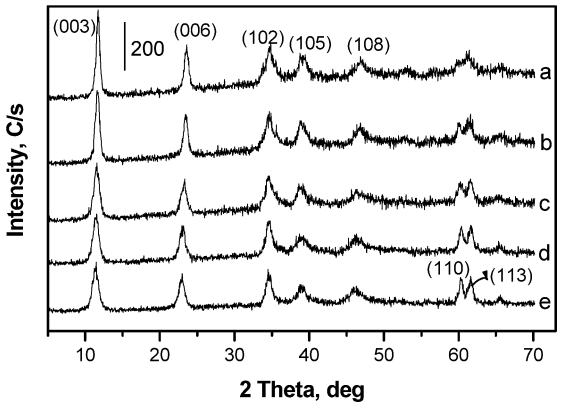

Fig. 1. Powder X-ray diffraction patterns of (a) CuMgAl-51; (b) CuMgAl-31; (c) CuMgAl-11; (d) CuMgAl-13; and (e) CuMgAl-15.

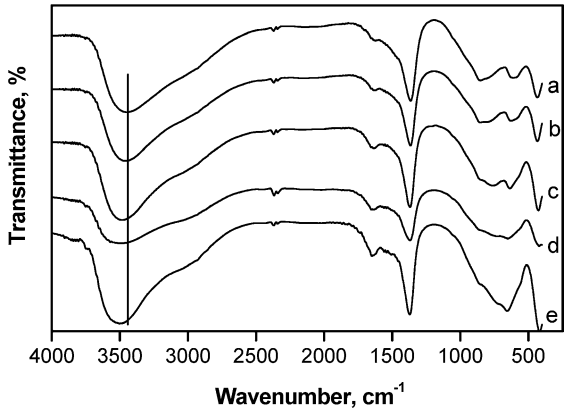

Fig. 2. FT-IR spectra of (a) CuMgAl-51; (b) CuMgAl-31; (c) CuMgAl-11; (d) CuMgAl-13; and (e) CuMgAl-15.

diffraction by basal planes (003), (006), and (009), respectively) and broad, less intense peaks at higher angles (peaks close to $2\theta = 38°$, 46°, and 60°; ascribed to diffraction by (105), (108), and (110) planes) confirm the presence of hydrotalcite (JCPDS: 41-1428) with 3R packing of layers [17]. The positions of the remaining peaks are in agreement with such an assignment. No significant positional changes in the basal or the *ab* plane reflections were noted with the variation in the Cu/Mg atomic ratio. This could possibly be explained by only subtle differences in the octahedral ionic radii of Cu^{2+} (0.73 Å) and Mg^{2+} (0.72 Å) [18]. However, a clear improvement in the orderliness of the layer was noted with decreasing copper content, as indicated by both the increase in intensity and sharpness of (110) and (113) reflections observed around 60° and 62°. This is expected, since at higher concentrations of copper a Jahn–Teller distortion is expected, leading to poor long-range ordering. Lattice parameters *a* and *c*, calculated from the (003), (006), and (110) reflections, are summarized in Table 1. Assuming a value of 4.8 Å for the width of brucite-like layers [19], the interlayer distance is close to 2.7–2.9 Å, suggesting the location of carbonate anions with their molecular planes parallel to the brucite-like layers.

FT-IR spectra for the samples are shown in Fig. 2. Although all samples show rather similar spectra, subtle differences can be noted. The main band is recorded around 3450–3500 cm^{-1} and is due to the ν_{OH} mode of H-bonded hydroxyl groups in the layers and of interlayer water molecules. The band becomes sharper and shifts toward higher wave numbers with an increase in magnesium concentration. This suggests that the strength of hydrogen bonding (through different kinds of interaction of OH species) is similar upon an increase in magnesium concentration. This is in accordance with PXRD results, which also implied a better long-range ordering (i.e., similar kind of M–OH point group arrangements in the lattice of the layered network). However, a shift toward higher wave numbers suggests an anomaly, as will be discussed later. This band shows a prominent shoulder around 2950 cm^{-1} ascribed to hydrogen bonding of hydroxyl groups of layered lattice and/or water molecules with interlayer carbonate anions [20]. A rather weak band at 1640 cm^{-1} is attributed to the deformation mode of interlayer water molecules whose intensity increased with increasing magnesium concentration, suggesting a higher content of water molecules, in accordance with the elemental composition results given in Table 1. A sharp band at 1370 cm^{-1} can be assigned to the antisymmetric ν_3 mode of interlayer carbonate anions. No shift of this band position is noted, regardless of the composition. It should further be noted that although the band is shifted from the position of free carbonate ($\sim$ 1450 cm^{-1}), it does not split. This fact, together with the absence of any band around 1050 cm^{-1} (position expected for the IR forbidden ν_1 mode of carbonate), suggests the retention of D_{3h} symmetry of the carbonate anion in the interlayers. Significant differences in the spectra were noted in the spectral region below 1000 cm^{-1} of M–OH stretching and M–OH–M′ bending vibrations due to compositional variations.

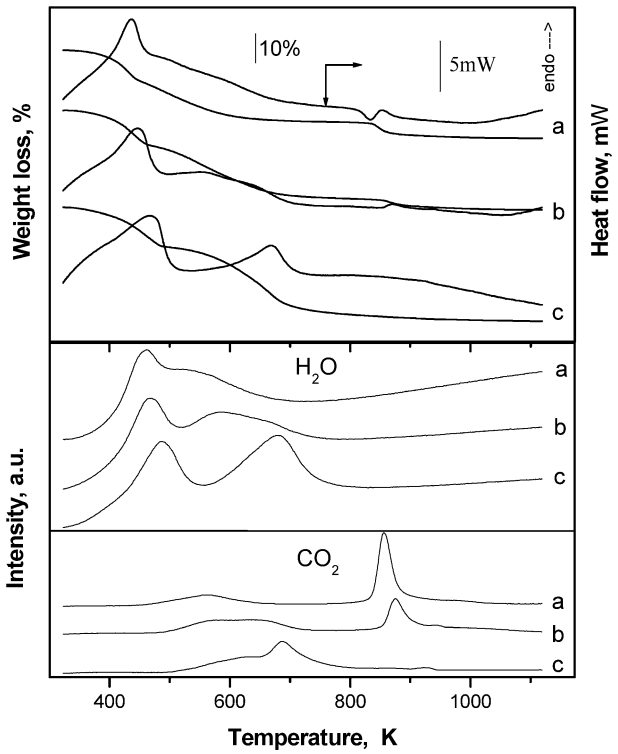

Fig. 3. TG-DTA traces and EGA traces (of water and CO_2) of (a) CuMgAl-51; (b) CuMgAl-11; and (c) CuMgAl-15.

Representative thermal analysis profiles of some of the samples are given in Fig. 3. Two well-defined weight losses were noted up to 773 K, which were duly complemented by two endotherms. However, the nature of the endotherms was different with the variation in the composition. For a copper-rich sample, the second endotherm or weight loss occurs in a broader temperature window, and a narrow endotherm was observed for a Mg-rich sample. The parallel analysis of the evolved gas (EGA) also supported the conclusion that the dehydration component of the second weight loss occurred in a wider temperature window for Cu-rich sam-

ples. Although EGA studies showed that the decarbonation temperature window becomes narrower with an increasing copper content, such a contribution of decarbonation to the peak shape is less significant compared with dehydroxylation. A sharper peak with single-stage evolution of carbonate (Fig. 3: CO_2: spectra a; considering up to 800 K) for a Cu-rich sample could suggest a similar nature and coordination of carbonate ion, preferably associated with Cu^{2+}. The two stages (whose temperatures are designated here by T_1 and T_2) are ascribed first to the removal of interlayer water molecules (transformation temperature T_1) and second to the dehydroxylation of brucite-like sheets and decarbonation (transformation temperature T_2) with concomitant destruction of the layer structure [21]. Furthermore, a progressive shift in the temperatures (both T_1 and T_2) to higher values was noticed as the magnesium concentration was increased. This is indeed expected, since magnesium is better stabilized in an octahedral coordination of a HT-like lattice than copper, which is inherently less stable in octahedral coordination because of Jahn–Teller distortion. However, these observations are in contrast with the results observed by FT-IR, wherein the strength of hydrogen bonding (considered a measure of interaction between layers and the interlayers) decreased with an increase in magnesium content (CuMgAl-15 $\nu_{OH} = 3496\ cm^{-1}$ and CuMgAl-51 $\nu_{OH} = 3450\ cm^{-1}$). In other words, dehydroxylation should be easier for the sample with weaker hydrogen bonding, that is, for a magnesium-rich sample, whereas the thermal analysis showed an opposite trend wherein T_2 increased with an increase in magnesium concentration. At this moment, the reason for such an observation is not clear.

In addition to these profiles, a well-defined endotherm was also noted around 823–873 K, whose weight loss contribution increased with an increase in copper concentration. A parallel attempt to study the evolved gases during thermal decomposition revealed the evolution of only CO_2, which suggests the presence of amorphous mixed oxycarbonate. A detailed thermal analysis pathway of Cu-containing hydrotalcites was recently reported [22].

Interesting information on the phase evolution of these materials emerged from an investigation made under in situ heating conditions by PXRD and DRIFT measurements. In situ PXRD of some selected samples is shown in Fig. 4. The diffraction patterns clearly indicate that the nature of the phase evolution is strongly influenced by the Cu/Mg atomic ratio. With an initial increase in temperature, a progressive decrease in the intensity of the basal reflections ((003) and (006)) occurs with a concomitant shift toward higher angles. This is attributed in general to the removal of interlayer water molecules, resulting in the shrinkage of interlayer space. A more detailed analysis of the diffraction patterns reveals that the complete decomposition of the HT-like lattice (as inferred by the disappearance of (003) reflection) shifted to higher temperatures with increasing magnesium concentration, that is, CuMgAl-51 at 523 K, CuMgAl-11 at 573 K, and CuMgAl-15 at 623 K. In other words, the stability of

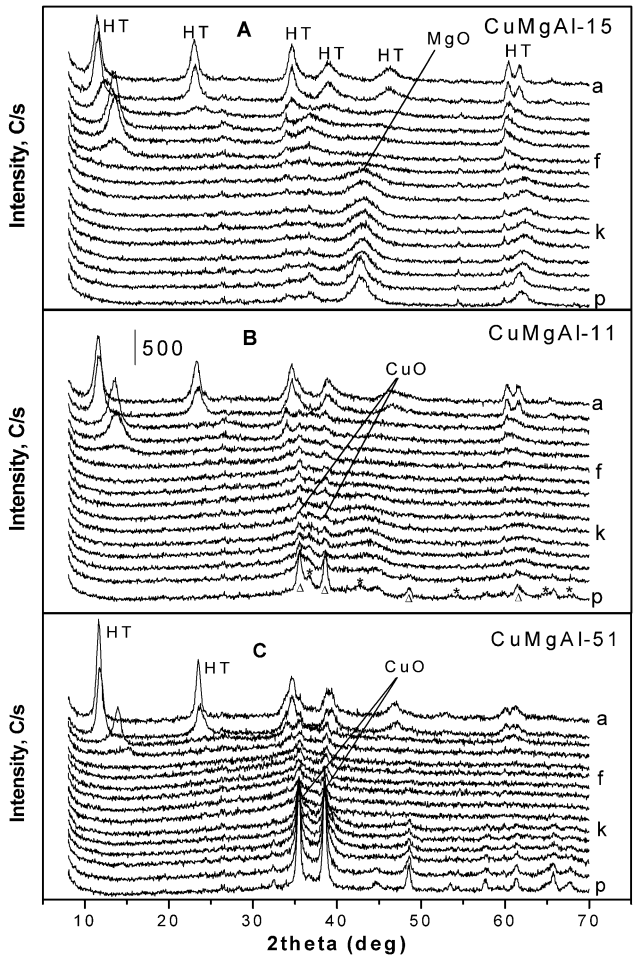

Fig. 4. In situ PXRD of CuMgAl-15, CuMgAl-11, and CuMgAl-51 calcined at (a) 323; (b) 373; (c) 423; (d) 473; (e) 523; (f) 573; (g) 623; (h) 673; (i) 723; (j) 773; (k) 823; (l) 873; (m) 923; (n) 973; (o) 1023; and (p) 1073 K (HT, hydrotalcite; △, CuO; ∗, spinel).

the HT-like lattice increased with the magnesium concentration, which is in accordance with TG-DTA results. With a further increase in temperature, crystallization of different phases occurs, the composition of which is influenced by chemical composition. In the case of CuMgAl-51, CuO forms, and its crystallinity is improved with increasing calcination temperature. However, above 823 K (Fig. 4C, k), crystallization of a spinel phase also occurs, the crystallinity of which improved with increasing temperature. From the chemical composition of this sample, this could possibly be $CuAl_2O_4$ with some partial substitution of magnesium (solid solution spinel). No discrete Mg-containing phase was observed in the entire temperature range studied. Interestingly, crystallization of CuO occurs at around 423 K, well below the T_1 temperature in the TG profile. Hence, formation of CuO occurs even when the layered structure prevails, suggesting that this formation might have occurred through dehydroxylation primarily along the edges of the layers. In contrast, the calcination of CuMgAl-15 showed the crystallization of a MgO phase, which was, however, very amorphous in nature, with a defect or nonstoichiom-

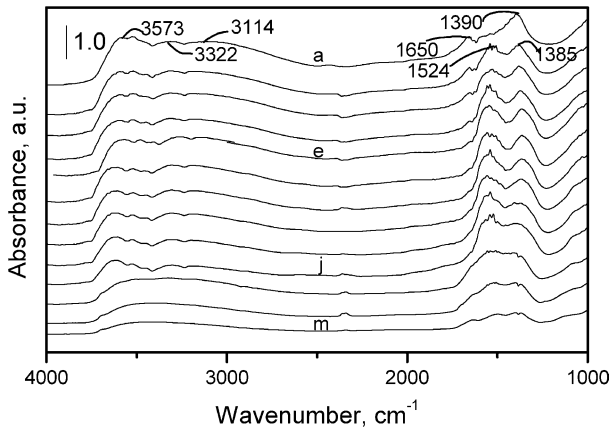

Fig. 5. In situ DRIFT spectra of CuMgAl-11 activated in air at (a) 303; (b) 323; (c) 373; (d) 423; (e) 473; (f) 523; (g) 573; (h) 623; (i) 673; (j) 723; (k) 773; (l) 873; (m) 973 K. (Ex situ calcined for 773, 873, and 973 K).

etry, as indicated by a significant displacement in the positions of the primary diffraction lines (Fig. 4A, h; $d_{(200)} = 2.092$ Å and $d_{(220)} = 1.482$ Å) with respect to synthetic periclase ($d_{(200)} = 2.110$ Å and $d_{(220)} = 1.490$ Å; JCPDS 45-0946). However, above 623 K, crystallization of MgO occurred, and the crystallinity of MgO increased (as indicated by the increase in sharpness and intensity of (200) and (220) reflections observed around 42° and 62°, respectively) with increasing temperature. However, regardless of the temperature, no crystalline discrete Cu-containing phase evolved, and no well-defined spinel phase was noted, even after heating at 1073 K. Hence, copper in this matrix might have been present in its oxidic form and well dispersed.

To complement this phase evolution process, we have also studied these samples by in situ DRIFT FT-IR measurements in air at increasing temperatures; representative spectra are given in Fig. 5. Because of limitations of the accessory attachment, the samples could be heated only to 773 K under in situ conditions, whereas spectra of samples calcined at higher temperature (> 773 K) were recorded ex situ. The spectrum at room temperature showed broad bands around 3500 cm^{-1} with shoulders at lower wavenumbers, indicating an extensive hydrogen-bonded hydroxy-water network. Bands were also noted around 1650 and 1380 cm^{-1}, which were assigned as above. Calcination of the sample at slightly elevated temperatures (e.g., 373 K) showed significant variations in the carbonate region, with the carbonate band splitting into two bands around 1530 and 1380 cm^{-1}. Such a split was noted earlier by us [23] and by Cabrera et al. [24] and ascribed to a change in the coordination of the carbonate ion upon loss of interlayer water molecules. In recent work [22], we reported the presence of unidentate coordination of carbonate with metal ions in the brucite-like lattice, based on the extent of such splitting. A further increase in temperature decreased the intensity of both ν_{OH} and δ_{H_2O} vibrations. However, samples showed weak vibrations of carbonate, even after calcination at 973 K, suggesting the presence of amorphous oxycarbonate.

Table 2
Phenol hydroxylation activity of CuMgAl ternary hydrotalcites[a]

Catalyst	Conversion (%)	Product distribution (wt%)			TON[b] (h^{-1})
		CAT	HQ	CAT/HQ	
CuMgAl-51	23.5	13.7	9.8	1.4	37
CuMgAl-31	24.7	16.5	8.2	2.0	46
CuMgAl-11	22.0	13.5	8.5	1.6	51
CuMgAl-13	19.1	13.0	6.1	2.1	95
CuMgAl-15	17.7	12.2	5.5	2.2	128

[a] Reaction conditions: phenol, 1.0 g; phenol/H_2O_2 molar ratio, 2.0; catalyst mass, 10 mg; solvent, water (10 ml); temperature, 338 K; time, 2 h.
[b] Moles of phenol converted per mole of copper per hour.

3.2. Catalytic hydroxylation of phenol

Table 2 summarizes the activity of these catalysts studied for phenol hydroxylation. On all catalysts, catechol (CAT) and hydroquinone (HQ) were observed as major products. Among the catalysts studied, CuMgAl-31 showed maximum activity with nearly 50% selectivity of H_2O_2 (selectivity is defined here on the basis of dihydroxybenzenes formed). Furthermore, the product distribution indicated a CAT/HQ ratio of around 2.0, unlike that obtained for CuCoAl catalysts [9], suggesting an influence of the nature of the second cation in controlling the course of the reaction. Binary MgAl hydrotalcite with a Mg/Al atomic ratio of 3.0 did not show any hydroxylation of phenol under similar reaction conditions. Hence, the presence of copper is essential for this reaction to occur. Although an attempt to synthesize a single-phase CuAl binary hydrotalcite failed as expected (because of the Jahn–Teller effect, a mixed phase containing gerhardite (or malachite) and hydrotalcite was obtained), this binary hydrotalcite also showed a conversion much lower than that of any of the ternary catalysts studied here, suggesting that the presence of both copper and magnesium augmented the activity. The activity was normalized and expressed as a turnover number (TON), which is defined as moles of phenol produced per mole of copper per hour. The TON values are also summarized in Table 2 and show an opposite trend (to that of actual conversion of phenol), with TONs increasing with increasing magnesium concentration. The dilution of copper by magnesium obviously enhances the specific activity of copper for the hydroxylation of phenol.

Fig. 6 illustrates the variation of the substrate/catalyst mass ratio with the phenol conversion for CuMgAl-51. As shown in the figure, the conversion of phenol increased with decreasing substrate/catalyst ratios at values above approximately 100 and then started decreasing at still lower substrate/catalyst ratios. This decrease is presumably due to spontaneous formation of coke (as indicated by the darker color of the reaction mixture) at higher catalyst concentrations, obtained through consecutive oxidation of primary products (catechol and hydroquinone). To verify the formation of coke, in one of our experiments we filtered the reaction mixture, and the solid was washed, dried, and sub-

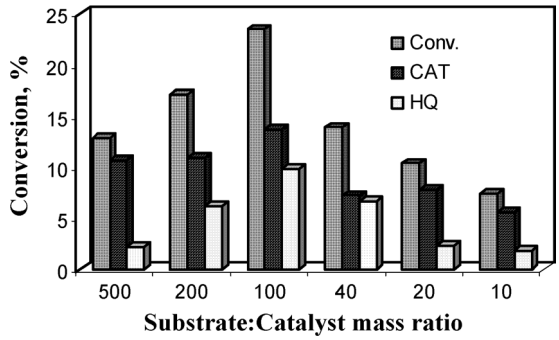

Fig. 6. Variation in conversion of phenol with the substrate:catalyst mass ratio for CuMgAl-51 (phenol, 1 g; solvent (water), 10 ml; phenol/H_2O_2 molar ratio, 2.0; temperature, 338 K; time, 2 h).

Table 3
Influence of reaction temperature on phenol hydroxylation over CuMgAl ternary hydrotalcites[a]

Catalyst	Temp. (K)	Conv. (%)	Product distribution (wt%)			H_2O_2 selec.[b] (%)
			CAT	HQ	CAT/HQ	
CuMgAl-51	303	18.5	11.0	7.5	1.5	37.0
	323	20.2	12.1	8.1	1.5	47.0
	338	23.5	13.7	9.8	1.4	47.0
	353	15.3	9.2	6.1	1.5	30.6
CuMgAl-31	303	20.1	12.0	8.1	1.5	40.2
	323	22.3	13.5	8.8	1.5	44.6
	338	24.7	16.5	8.2	2.0	49.4
	353	17.0	11.0	6.0	1.8	34.0
CuMgAl-11	303	17.2	11.7	5.5	2.1	34.4
	323	20.0	13.8	7.2	1.9	40.0
	338	22.0	13.5	8.5	1.6	44.0
	353	14.0	8.2	5.8	1.4	28.0

[a] Reaction conditions as in Table 2.
[b] Selectivity of H_2O_2 calculated on the basis of dihydroxybenzenes formed.

jected to heating in air at 550 °C. A significant difference in the weight was noted between the as-filtered solid and the heated sample (10–13 mg of coke after the weight loss due to hydrotalcite is taken into consideration), corroborating the formation of coke, which is oxidized after heating in air. Similar observations were also made earlier for both CuNiAl and CuCoAl ternary hydrotalcites [9]. In addition, a preferential formation of catechol was noted at both extremes of substrate:catalyst ratios, suggesting the hindrance of interconversion and/or isomerization reactions. A substrate/catalyst ratio of 100 was selected for all further studies.

Table 3 shows the variation in the catalytic performance with reaction temperature over some of the catalysts studied. A subtle increase in the conversion was noted up to 338 K, whereas a further increase in temperature reduced the conversion of phenol; this could be ascribed to competitive thermal decomposition of H_2O_2 at higher temperature. However, the CAT/HQ ratio was not influenced by the reaction temperature, and the decrease in the conversion between 338 and 353 K occurred with all catalysts. An analysis com-

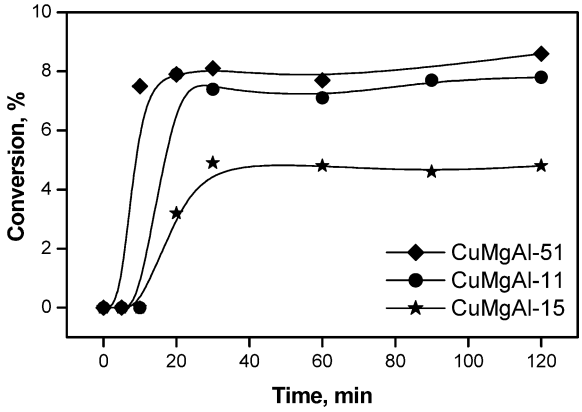

Fig. 7. Influence of reaction time on the phenol conversion (phenol, 1 g; substrate:oxidant molar ratio, 5:1; temperature, 338 K; solvent (water), 10 ml; substrate:catalyst mass ratio, 100).

paring these results with those obtained for CuCoAl and CuNiAl ternary hydrotalcites showed a characteristic trend in that the activity of CuMgAl ternary hydrotalcites at room temperature was significantly higher than that of any other catalyst studied so far, suggesting the influence of the second divalent metal ion. For example, a conversion as high as 20% was noted at room temperature (303 K) for CuMgAl-31 for a substrate/oxidant mole ratio of 2:1. Such high activity could be due to better stabilization of Cu^{2+} in the octahedral sites of the CuMgAl HT-like lattice.

To study the influence of the reaction medium on phenol hydroxylation, the reaction was performed in various solvents (other than water), namely, acetone, acetonitrile, *t*-butanol, THF, and dimethylformamide (DMF). In none of these solvents was measurable conversion of phenol observed. We believe that the proximity of the hydroxylating species and the substrate molecule on the surface is essential; the corresponding configuration would be well stabilized in H_2O. In water, both phenol and H_2O_2 dissolve simultaneously and can approach the active center, thereby generating the hydroxyl radicals, thought to be the active species involved in the hydroxylation reaction. Furthermore, when the reaction was carried out with oxidants other than H_2O_2, namely, oxygen, air, and *t*-butylhydroperoxide, no conversion was detected under similar conditions. This could possibly be due to the lack of generation of active oxygen species and solubility problems associated with the reactant and oxidant.

Fig. 7 shows the variation in the conversion of phenol over some of the catalysts studied at different time intervals with a substrate/oxidant mole ratio of 5:1. This ratio was selected to evaluate these catalysts at low conversion levels. It is clear from the figure that more than 90% of the total conversion was achieved in less than 30 min, but a further increase in time did not change the conversion significantly. A small induction period of 5–10 min was noted for these catalysts. This is in contrast to the behavior of many zeolite-based catalysts, which either show a progressive growth in the conversion of phenol or exhibit an induc-

tion period [25]. No significant variation in the CAT/HQ ratio was noticed with time, suggesting the absence of interconversion and/or consecutive reactions. In other words, the hydroxylation of phenol over these catalysts occurs in parallel mode in forming catechol and hydroquinone simultaneously. As a test for possible contributions of a homogeneous reaction, CuMgAl-51 was suspended in H_2O_2 at 338 K for 30 min. The solid was then separated and the filtrate tested for phenol hydroxylation with a substrate/oxidant ratio of 2:1. A conversion of only ca. 3–4% with selective formation of catechol was measured after 2 h of reaction. This conversion is much smaller than that observed in the presence of the solid catalyst (23.5% with a CAT/HQ ratio of 1.4), suggesting that contributions of homogeneous reactions catalyzed by leached metal ions were essentially absent. Variations in the substrate/oxidant molar ratios indicated that the conversion increased with a decrease in the ratio, the values of which are summarized in Table 4. A continuous increase in the selectivity of H_2O_2 was noted with an increase in the substrate/oxidant mole ratio of up to 2:1, whereas a further increase in this ratio decreased its selectivity. It is commonly noted, even for the systems studied earlier by us, that at high concentrations of H_2O_2 the contribution of undesired consecutive reactions may dominate, thereby reducing the overall selectivity for the desired products [8,10]. In addition, a selectivity for catechol was noted at higher H_2O_2 concentration, suggesting a varied kinetic dependence of H_2O_2 concentration on the nature of dihydroxybenzene formed. The reusability of the catalysts was checked and it was found that the activity dropped with cycle time. For instance, CuMgAl-51 showed 23.5% conversion with a CAT/HQ ratio of 1.4 in the first run in 2 h, 16% in the second cycle, 9% in the third, and 5% in the fourth, with selective formation of catechol, however, in 24 h for all subsequent cycles. Between the cycles, the catalyst was filtered and washed thoroughly with water, dried, and re-used (catalyst weight loss due to handling was taken into consideration while fixing the reaction variables). The drop in the activity was attributed to loss in the crystallinity of the sample upon reaction, as indicated by PXRD. We had made such an observation earlier for CoNiAl ternary systems for the hydroxylation of phenol [8].

To test the catalytic performance for the hydroxylation of phenol of mixed-metal oxides derived from HT-like precursors, some of these materials were calcined at different temperatures (423, 673, 873, and 1073 K) for 6 h and then screened for hydroxylation of phenol (Table 5). The calcination temperatures were chosen based on TG results so as to cover different stages of thermal decompositions. In the case of CuMgAl-51, no significant change in the conversion was noted, regardless of the calcination temperature, whereas in the case of CuMgAl-11 a subtle increase in the conversion was observed with increasing temperature. This could possibly be caused by a better dispersion of CuO in the magnesium oxide matrix in the case of the latter material, whereas agglomeration is more prominent in the case of the former. This is in accordance with the in situ PXRD results (Fig. 4) mentioned earlier, which showed that the crystallinity of the CuO was better for CuMgAl-51 as compared with CuMgAl-11. Furthermore, a difference in the CAT/HQ ratio was also detected for these two calcined catalysts, suggesting that the CuO dispersion is influencing the course of the reaction [26]. However, it should be noted here that the activity of calcined catalysts was less than that of their corresponding uncalcined forms, regardless of the calcination temperature.

Table 4
Effect of the substrate:oxidant molar ratio (Sub/Oxi) for phenol hydroxylation over CuMgAl ternary hydrotalcites[a]

Catalyst	Sub/Oxi	Conv. (%)	Product distribution (wt%)			H_2O_2 selec.[b] (%)
			CAT	HQ	CAT/HQ	
CuMgAl-51	10:1	1.8	1.8	0	–	18.0
	5:1	6.1	5.1	1.0	5.1	30.5
	3:1	9.7	6.7	3.0	2.2	29.1
	2:1	23.5	13.7	9.8	1.4	47.0
	1:1	37.1	33.7	3.4	9.8	37.1
	1:2	55.7	51.5	4.2	12.2	27.8
CuMgAl-31	10:1	2.9	2.9	0	–	29.0
	5:1	4.3	4.3	0	–	21.5
	3:1	11.3	8.0	3.3	2.4	33.9
	2:1	24.7	16.5	8.2	2.0	49.4
	1:1	43.9	31.2	12.7	2.5	43.9
	1:2	59.5	48.2	11.3	4.3	29.8
CuMgAl-11	10:1	2.1	2.1	0	–	21.0
	5:1	7.1	5.2	1.9	2.7	35.5
	3:1	12.4	7.0	5.4	1.3	37.2
	2:1	22.0	13.5	8.5	1.6	44.0
	1:1	38.2	30.0	8.2	3.7	38.2
	1:2	65.0	50.2	14.8	3.4	32.5

[a] Reaction conditions: phenol, 1.0 g; catalyst, 10 mg; solvent, water (10 ml); temperature, 338 K; time, 2 h.
[b] Selectivity of H_2O_2 calculated on the basis of dihydroxybenzenes formed.

Table 5
Influence of calcination temperature on phenol hydroxylation over CuMgAl catalysts[a]

Catalyst	Calcination temp. (K)	Conv. (%)	Product distribution (wt%)			H_2O_2 selec.[b] (%)
			CAT	HQ	CAT/HQ	
CuMgAl-51	423	16.2	12.2	4.0	3.1	32.4
	673	17.9	13.7	4.2	3.3	35.8
	873	16.3	12.1	4.2	2.9	32.6
	1073	18.6	13.0	5.6	2.3	37.2
CuMgAl-31	423	18.5	14.9	3.6	4.1	37.0
	673	20.9	14.4	6.5	2.2	41.8
	873	20.5	14.3	6.2	2.3	41.0
	1073	18.6	13.0	5.6	2.3	37.2
CuMgAl-11	423	15.2	9.3	5.9	1.6	30.4
	673	18.2	14.2	4.0	3.6	36.4
	873	19.7	12.1	7.6	1.6	39.4
	1073	19.0	11.0	8.0	1.4	38.0

[a] Reaction conditions as in Table 2.
[b] Selectivity of H_2O_2 calculated on the basis of dihydroxybenzenes formed.

Table 6
Specific surface areas and pore parameters of CuMgAl ternary hydrotalcites

Catalyst	Surface area ($m^2\ g^{-1}$)	Pore volume[a] ($cm^3\ g^{-1}$)	Average pore size[a] (Å)
CuMgAl-51	62	0.50	260
CuMgAl-31	74	0.51	220
CuMgAl-11	114	0.72	180
CuMgAl-13	125	0.91	200
CuMgAl-15	130	0.90	200

[a] Calculated based on desorption branch of isotherm.

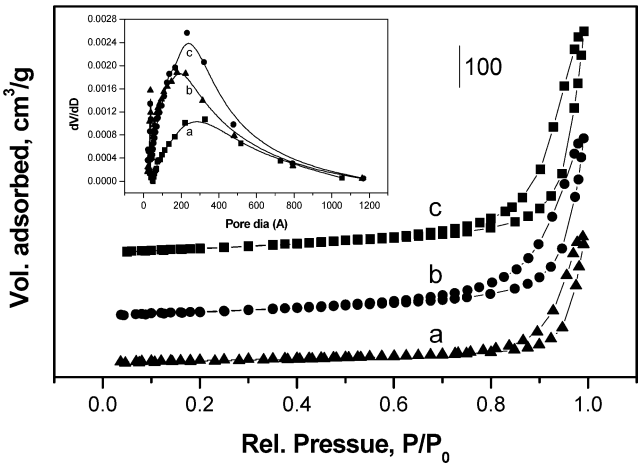

Fig. 8. N_2 adsorption isotherms at 77 K of (a) CuMgAl-51; (b) CuMgAl-11; and (c) CuMgAl-15 (isotherms (b) and (c) are displaced vertically for clarity). Inset: Pore size distribution (BJH, desorption branch of isotherm).

3.3. Structure–activity correlations

From these discussions it is quite clear that copper is indeed an essential component in the catalyst, without which the phenol hydroxylation is not catalyzed. It is interesting to discuss the reasons for the dependence of the phenol hydroxylation on the copper concentration in the CuMgAl ternary HT-like lattice. The results discussed above demonstrate that catalysts containing low concentrations of copper, such as CuMgAl-15, exhibit the highest specific activities of copper, suggesting that isolated copper centers possess the highest intrinsic activity. Moreover, the ternary catalysts develop increasing BET surface areas as the magnesium content increases. Surface areas are summarized in Table 6. Dinitrogen adsorption isotherms at 77 K for CuMgAl-51, CuMgAl-15, and CuMgAl-11 are shown in Fig. 8. They show the type II pattern of the IUPAC classification [27] with a rather small hysteresis loop (type B), the area of which increases with increasing magnesium content. The loops close at a relative pressure of 0.7–0.8 for all three samples, indicating a similar pore architecture of largely mesoporous dimensions. In other words, the interlayer space is inaccessible for nitrogen molecules. These results are further corroborated by the pore size distribution of these samples, shown as an inset in Fig. 8. In general, pore formation in hydrotalcites is through interparticle packing, and the distribution of pores is influenced by the crystallite size and packing arrangement of crystallites [2]. A relatively narrow distribution of pores was observed for CuMgAl-15, whereas a broader distribution of pores prevails for CuMgAl-51. This is indeed reflected in the BJH pore diameter of these samples (computed from the desorption branch of the isotherm). The former had an average pore diameter (derived from the desorption branch of the isotherm) of 200 Å, and the latter showed 260 Å, and with the specific surface area of the former was twice that of the latter. This could possibly be due to the better orderliness of crystallites, as indicated by PXRD for CuMgAl-15. The total pore volume, specific surface area, and the area of the hysteresis loop increases with an increase in magnesium content. These changes probably originate from morphological differences in the crystallites arising with a change in magnesium concentration. In anticipation of finding such differences, scanning electron microscopy was carried out for some of these samples; the results are shown in Fig. 9. At first glance the micrographs would indicate that all samples consist of platelets; however, overlapping of such platelets occurs, thereby exhibiting a kind of spongy morphology. However, a closer look at the micrographs clearly shows that the extent of agglomeration decreased with increasing magnesium concentration. In other words, for sample CuMgAl-51, platelet agglomeration occurs strongly in forming such spongy particles 3–15 μm in diameter, whereas CuMgAl-15 consists of particles of 1–3 μm. This is presumably in accordance with pore size distribution results wherein contributions of larger pores were formed in greater numbers through interparticles for CuMgAl-51. In other words, the prevalence of an ordered lattice at higher magnesium concentration (smaller particle size), coupled with the larger surface area, offers higher dispersion of copper and hence exhibits higher intrinsic activity. It has generally been observed that the electronic properties of the metal ions change subtly with changes in their dispersion [28]. In anticipation of such behavior, UV–vis spectra of these samples were measured; these are shown in Fig. 10. All samples showed rather similar spectra exhibiting two bands in the region near 750 and 250 nm. The first band is generally ascribed to d–d transitions, and the second band is attributed to charge transfer transitions (CT). A continuous drop in the integral intensities of both bands is in accordance with the decrease in the concentration of copper. Subtle differences are noted in the peak positions for both transitions with changing Cu/Mg atomic composition. A progressive shift to lower wavelengths was noted for the d–d transition with increasing concentration of copper, which is inferred to suggest a decrease in dispersion. This is in accordance with the results of Marion et al. [29], who studied the variation in spectral features with the variation of the copper content and aging in a methane–air reaction mixture over Cu/Al_2O_3 catalysts. The peak around 250 nm could be specifically attributed to an $O^{2-} \rightarrow Cu^{2+}$ charge transfer transition. The energy of the transition depends on the symmetry, oxidation state of the metal ion, and the nature of the ligand or of the other metal atom [30]. In general, the energy of the CT band increases with the optical

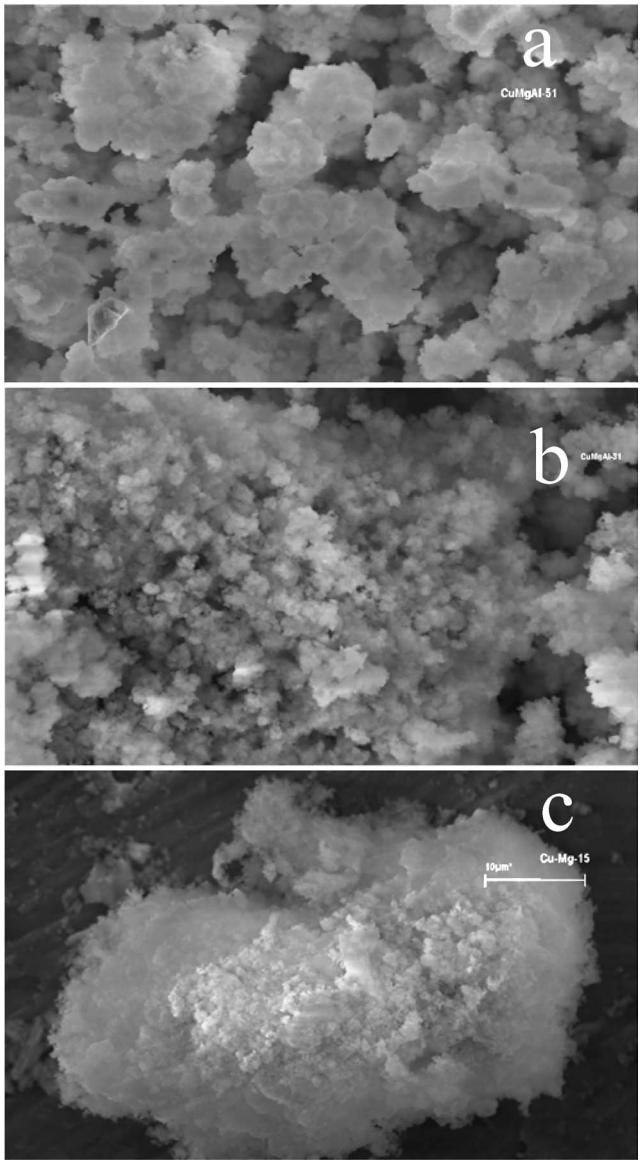

Fig. 9. Scanning electron micrographs of (a) CuMgAl-51; (b) CuMgAl-11; and (c) CuMgAl-15.

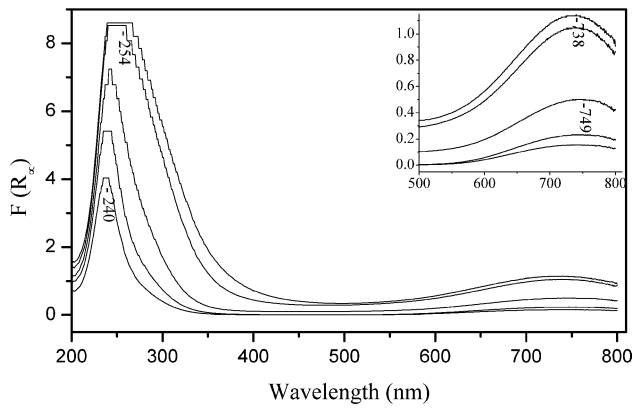

Fig. 10. UV–vis diffuse reflectance (SKM function) spectra of (a) CuMgAl-51; (b) CuMgAl-31; (c) CuMgAl-11; (d) CuMgAl-13; and (e) CuMgAl-15 (top a and bottom e); inset: ordinate expanded region of d–d transition.

electronegativity difference between metal and ligand [31]:

$$\nu_{CT} = 30{,}000\left(\chi_{opt}(L) - \chi_{opt}(M)\right)\ \mathrm{cm}^{-1}$$

for ligand-to-metal charge transfer (LMCT), where χ_{opt} (L) and χ_{opt} (M) are the optical electronegativities of the donor and acceptor orbitals on the ligand and metal, respectively. In our series of catalysts, a continuous increase in the energies of the charge transfer transition was noted (CuMgAl-51 = 39,370 cm^{-1}; CuMgAl-15 = 41,720 cm^{-1}) with an increase in magnesium concentration. Based on the equation given above, the optical electronegativity of the metal ion decreases with an increase in magnesium concentration. Here it is assumed that there is a negligible change in the nature of the ligand (namely oxygen in the form of OH) and its coordination in the HT-like lattice. In other words, the ease of oxidation of Cu^{2+} increases with a decrease in its concentration in the CuMgAl HT-like lattice and hence shows higher intrinsic activity.

These results are further corroborated by cyclic temperature-programmed reduction–reoxidation (TPRO) measurements. Data for selected samples are shown in Fig. 11. It must be admitted that these experiments were performed for catalyst samples after/during heating (i.e., after the destruction of the layered structure), whereas catalysis was done with uncalcined layered materials. The analysis of the redox behavior of these materials, however, may add to the understanding of the properties of these materials. Temperature-programmed reduction and reoxidation were done in a cyclic form, in which the uncalcined hydrotalcite was subjected to reduction during heating in the first step, and the resulting reduced matrix was then subjected to reoxidation. During the second cycle, the oxidized form, present as a mixed-metal oxide, was subjected to reduction (at this stage there was no prevalence of a HT-like phase), and the reduced species was subjected to reoxidation. Due care was taken to have the characteristic K number around 100, well within the range suggested by Monti and Baiker, where K is given by the formula $K = n_0/FC_o$, where n_0 is the initial amount of reducible species in μmoles, F is the flow rate of the reducing gas mixture in $\mathrm{cc\,s}^{-1}$, and C_o is the concentration of reductant in $\mu\mathrm{mol\,cc}^{-1}$. In the first reduction profile, a two-stage reduction occurs at around 560 and 600 K; however, the intensity of the former peak decreases with a decrease in copper concentration (Fig. 11A). This peak may be assigned to reduction of CuO formed through dehydroxylation of a HT-like network to Cu^0 [32]. In addition, there were high temperature peaks of low intensity for the sample with low copper concentration, the intensity of which increased with a decrease in copper content. This could tentatively be explained by in situ generation of some nonstoichiometric CuO (which may also be present as nonstoichiometric spinel solid solution), which reduced at a relatively higher temperature. Such a formation may be favorable when copper is present in a well-dispersed form. Reoxidation of this sample in oxygen revealed a similar two-stage reoxidation profile (Fig. 11B); however, the temperature of reoxidation shifted

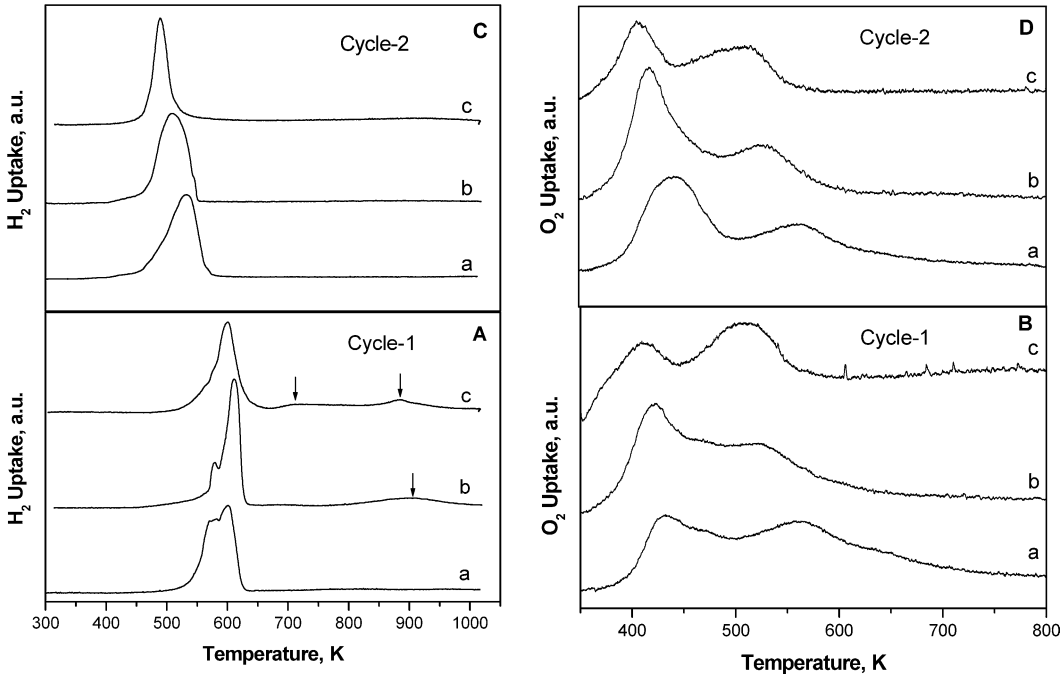

Fig. 11. Temperature-programmed reduction–reoxidation traces of (a) CuMgAl-51; (b) CuMgAl-11; and (c) CuMgAl-15. The samples were first reduced (Cycle 1—TPR; graph A), then oxidized (Cycle 1—TPO; graph B) and the oxidized sample is then re-reduced (Cycle 2—TPR; graph C) and the sample is then re-oxidized (Cycle 2—TPO; graph D).

to lower temperatures with a decrease in copper content, suggesting better oxidizability for the sample with a low copper concentration. The second cycle of this sample showed a single peak reduction pattern with no high temperature features for any of the samples (Fig. 11C). The temperature of reduction, T_R (here again CuO to Cu), shifted to lower temperatures with decreasing copper concentration. The cyclic oxidation showed a reoxidation profile similar to that for the first cycle (Fig. 11D). In conclusion, the cyclic TPRO measurements provide clues for the better redox behavior (as inferred from T_R) for the sample with low concentration of copper, and, hence, better intrinsic catalytic activity is inferred. These results are further complemented by X-ray photoelectron spectroscopy (XPS). Cu 2p XP spectra for some of the samples are shown in Fig. 12. The presence of shake-up satellite features for both Cu $2p_{3/2}$ and Cu $2p_{1/2}$ indicated that copper is predominantly present on the surface as Cu^{2+}. In addition, a decrease in the intensity was noted with decreasing copper concentration. The surface compositional analysis (Table 7) showed an enrichment of aluminum in accordance with the results of Corma and co-workers [33], with a surface (Cu + Mg)/Al ratio much lower than that in the bulk (a value close to 1.0 was noted for surface (Cu + Mg)/Al for these samples, whereas the bulk value was 3.0). Enrichment in magnesium was also noted; however, it depended on its bulk concentration. A closer look at the spectra would suggest a shift in the binding energy E_b to lower values with an increase in magnesium concentration (CuMgAl-51: 933.4 eV; CuMgAl-15: 932.6 eV). The lower binding energy for CuMgAl-15 may suggest easier oxidizability. Furthermore, the ratios of satellite to main peaks (I_s/I_m) were calculated for these samples; these are summarized in Table 7. They showed a progressive decrease with an increase in magnesium concentration, suggesting a varying

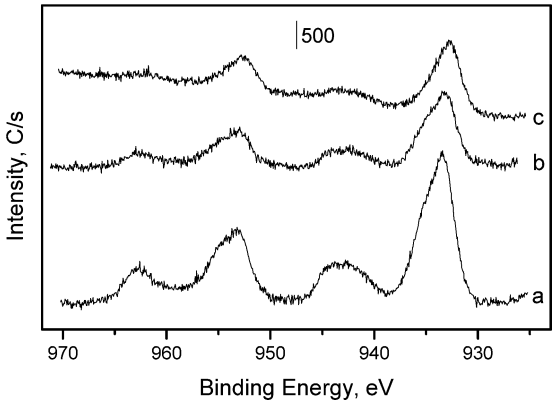

Fig. 12. Cu 2p X-ray photoelectron spectra of (a) CuMgAl-51; (b) CuMgAl-11; and (c) CuMgAl-15.

Table 7
XP spectral parameters of CuMgAl ternary hydrotalcites

Sample	E_b(Cu $2p_{3/2}$) (eV)	(Cu + Mg)/Al atomic ratio[a]	Cu/Mg atomic ratio[a]	I_s/I_m
CuMgAl-51	935.2, 933.4	0.99	2.49	0.38
CuMgAl-31	933.9	1.05	1.63	0.49
CuMgAl-11	933.2	1.02	0.59	0.37
CuMgAl-13	932.8	1.00	0.20	0.13
CuMgAl-15	932.6	0.86	0.14	0.13

[a] On surface.

charge density of copper atoms, although they are present in a similar HT-like lattice. The lower value of I_s/I_m for CuMgAl-15 may suggest a facile reducibility of Cu^{2+}. It is inferred that the facile redox behavior of this sample facilitates the oxidation reaction and in turn exhibits high intrinsic activity.

4. Conclusions

CuMgAl ternary hydrotalcites with different Cu/Mg atomic compositions were successfully synthesized in the entire composition range studied (from 5.0 to 0.2) without co-crystallization of any impurity phases. The orderliness of the HT-like lattice and the thermal stability of these materials increased with increasing magnesium concentration. Activity for selective hydroxylation of phenol with H_2O_2 as oxidant and H_2O as solvent increased with increasing copper concentration, whereas normalized activity showed a reverse trend. A mixed trend in the activity was noted with the variation in the substrate/catalyst ratio. Comparison of the activity of as-synthesized hydrotalcites with their corresponding calcined forms indicated that the former are more active than the latter. A variation in the activity trend was noted when compared among the calcined samples, which was due to varied phase compositions (influenced by the Cu/Mg atomic ratio, as indicated by in situ PXRD). The better intrinsic activity for the sample with a lower copper content is caused by better dispersion of the active metal ion, here Cu^{2+}, and its facile redox behavior, as indicated by N_2 adsorption measurements, cyclic TPRO, SEM, and spectroscopic measurements.

Acknowledgments

S.K. thanks the Alexander von Humboldt Foundation, Bonn, Germany, for a research fellowship. S.K also thanks the Council of Scientific and Industrial Research, New Delhi, India, for a research fellowship under the Young Scientist Scheme. The authors also thank the referees for their constructive criticism, which has definitively improved the quality of this paper.

References

[1] F. Trifirò, A. Vaccari, in: J.L. Atwood, J.E.D. Dasvies, D.D. MacNicol, F. Vogtle, J.-M. Lehn, G. Alberti, T. Bein (Eds.), Comprehensive Supramolecular Chemistry, Solid State Supramolecular Chemistry: Two and Three-Dimensional Inorganic Networks, vol. 7, Pergamon, Oxford, 1996, p. 251.
[2] V. Rives, Layered Double Hydroxides: Present and Future, Nova Sci. Pub. Inc., New York, 2001.
[3] K. Koteswara Rao, M. Gravelle, J.-S. Valente, F. Figueras, J. Catal. 173 (1998) 115.
[4] B.M. Choudary, M. Lakshmi Kantam, A. Rahman, V.Ch. Reddy, K. Koteswara Rao, Angew Chem. Int. Ed. 40 (2001) 763.
[5] D. Tichit, B. Coq, CATTECH 7 (2003) 206.
[6] S. Narayanan, K. Krishna, Appl. Catal. A 198 (2000) 13.
[7] R. Kalouskova, M. Novotna, Z. Vymazal, Polymer Degrad. Stability 85 (2004) 903.
[8] V. Rives, O. Prieto, A. Dubey, S. Kannan, J. Catal. 220 (2003) 161.
[9] A. Dubey, V. Rives, S. Kannan, Phys. Chem. Chem. Phys. 3 (2001) 4826.
[10] A. Dubey, V. Rives, S. Kannan, J. Mol. Catal. A 181 (2002) 151.
[11] I.J. Shannon, F. Rey, G. Sankar, J.M. Thomas, T. Maschmeyer, A.M. Waller, A.E. Palomares, A. Corma, A.J. Dent, G.N. Greaves, J. Chem. Soc. Faraday Trans. 92 (1996) 4331.
[12] S.M. Auer, S.V. Gredig, R.A. Koppel, A. Baiker, J. Mol. Catal. 141 (1999) 193.
[13] M. Trombetta, G. Ramis, G. Busca, B. Monanari, A. Vaccari, Langmuir 13 (1997) 4628.
[14] K. Iwai, T. Yamauchi, K. Hashimoto, T. Mizugaki, K. Ebitani, K. Kaneda, Chem. Lett. 58 (2003).
[15] Joint Committee on Powder Diffraction Standards, International Centre for Diffraction Data, Pennsylvania, 1996 (Set No. 46).
[16] D.A.M. Monti, A. Baiker, J. Catal. 83 (1983) 323.
[17] A. De Roy, C. Forano, K. El Malki, J.P. Besse, in: M.L. Occelli, H. Robson (Eds.), Expanded Clays and Other Microporous Solids, Synthesis of Microporous Materials, Van Nostrand Reinhold, New York, 1992, chap. 7, p. 108.
[18] R.D. Shannon, C.T. Prewitt, Acta Crystallogr. B 25 (1969) 925.
[19] F.M. Labajos, V. Rives, M.A. Ulibarri, J. Mater. Sci. 27 (1992) 1546.
[20] J. Perez-Ramirez, G. Mul, J.A. Moulijn, Vibr. Spectrosc. 27 (2001) 75.
[21] W.T. Reichle, CHEMTECH 16 (1986) 58.
[22] S. Kannan, V. Rives, H. Knozinger, J. Solid State Chem. 177 (2004) 319.
[23] S. Kannan, Tz. Venkov, K. Hadjiivanov, H. Knozinger, Langmuir 20 (2004) 730.
[24] I. Melian-Cabrera, M.L. Granados, J.L.G. Fierro, Phys. Chem. Chem. Phys. 4 (2002) 3122.
[25] A. Germain, M. Allian, F. Figueras, Catal. Today 32 (1996) 145.
[26] S. Velu, K. Suzuki, M. Okazaki, M.P. Kapoor, T. Osaki, F. Ohashi, J. Catal. 194 (2000) 373.
[27] B.C. Lippens, J.H. de Boer, J. Catal. 4 (1965) 319.
[28] J.G. Nunan, P.B. Himelfarb, R.G. Herman, K. Klier, C.E. Bogdan, G.W. Simmons, Inorg. Chem. 28 (1989) 3868.
[29] M.C. Marion, E. Garbowski, M. Primet, J. Chem. Soc. Faraday Trans. 86 (1990) 3027.
[30] M. Che, F. Bozon-Verduraz, in: G. Ertl, H. Knozinger, J. Weitkamp (Eds.), Handbook of Heterogeneous Catalysis, vol. 2, Wiley–VCH, Weinheim, 1997, p. 642.
[31] A.B.P. Lever, Inorganic Electronic Spectroscopy, third ed., Elsevier, Amsterdam, 1997.
[32] A. Alejandre, F. Medina, P. Salagre, X. Correig, J.E. Sueiras, Chem. Mater. 11 (1999) 939.
[33] F. Marquez, A.E. Palomares, F. Rey, A. Corma, J. Mater. Chem. 11 (2001) 1675.